

TOPICAL REVIEW • OPEN ACCESS

Structure and reactivity of model CeO₂ surfaces

To cite this article: David C Grinter and Geoff Thornton 2022 *J. Phys.: Condens. Matter* **34** 253001

View the [article online](#) for updates and enhancements.

You may also like

- [Peer review statement](#)
- [Peer review statement](#)
- [Conference Information](#)

Topical Review

Structure and reactivity of model CeO₂ surfaces

David C Grinter¹  and Geoff Thornton^{2,*} ¹ Diamond Light Source, Harwell Science and Innovation Campus, Didcot OX11 0DE, United Kingdom² Department of Chemistry and London Centre for Nanotechnology, University College London, London WC1H 0AJ, United KingdomE-mail: g.thornton@ucl.ac.uk

Received 11 November 2021, revised 17 January 2022


Accepted for publication 14 March 2022

Published 20 April 2022

**Abstract**

As a key component in many industrial heterogeneous catalysts, the surface structure and reactivity of ceria, CeO₂, has attracted a lot of attention. In this topical review we discuss some of the approaches taken to form a deeper understanding of the surface physics and chemistry of this important and interesting material. In particular, we focus on the preparation of ultrathin ceria films, nanostructures and supported metal nanoparticles. Cutting-edge microscopic and spectroscopic experimental techniques are highlighted which can probe the behaviour of oxygen species and atomic defects on these model surfaces.

Keywords: ceria, STM, XPS, AP-XPS, XAS, heterogeneous catalysis

 Supplementary material for this article is available [online](#)

(Some figures may appear in colour only in the online journal)

1. Introduction


Ceria (cerium dioxide) is a key component of many heterogeneous catalyst systems with wide-ranging applications in critical industrial processes including water-gas-shift, methanol synthesis, methane reforming, and CO oxidation [1–6]. In addition to its role in catalysis, ceria also has important applications in solid oxide fuel cells and in optical and electronic devices [7–9].

A major reason for the catalytic activity of ceria is its ability to switch easily between the Ce⁴⁺ and Ce³⁺ oxidation states, which enables it to store and release oxygen during the course of reactions [10, 11]. This variability in oxygen stoichiometry is reflected in the structure of the ceria surface. This will be

illustrated and discussed in the course of this topical review, which summarises our work in this area in the context of the field in general.

In heterogeneous catalysts, ceria is usually employed as a support material for various active metal particles, stabilising them under often quite extreme temperatures and pressures. The local structure of the ceria surface is vital to this and will also be examined in this work. Bulk CeO₂ is insulating and as such often suffers from unwanted charging problems when interrogated using electron-based experimental techniques. As a result, it has become common to study ceria surfaces via the formation of ultrathin films, generally a few nm thick, supported on a metal single crystal surface. If the dimensionality of the ceria is further constrained by preparing islands of oxide supported on a catalytically active metal, a so-called ‘inverse model catalyst’ is formed. This allows access to the metal–ceria interface, which has uncovered novel behaviour in some instances, in particular involving spillover processes [12–14].

* Author to whom any correspondence should be addressed.

 Original content from this work may be used under the terms of the [Creative Commons Attribution 4.0 licence](#). Any further distribution of this work must maintain attribution to the author(s) and the title of the work, journal citation and DOI.

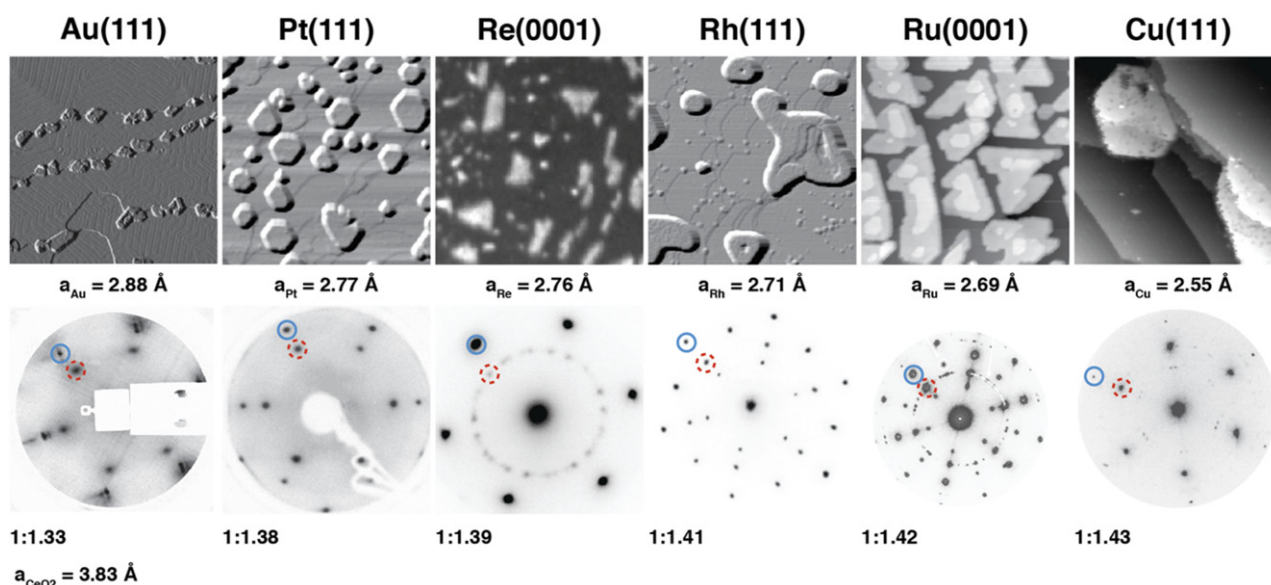


Figure 1. Micrographs (STM and low energy electron microscopy (LEEM) images, $200 \times 200 \text{ nm}^2$) and accompanying LEED patterns of $\text{CeO}_2(111)$ surfaces prepared on different supports. The ratio of the metal to CeO_2 lattice constants are indicated. Reprinted with permission from [12]. Copyright (2016) American Chemical Society.

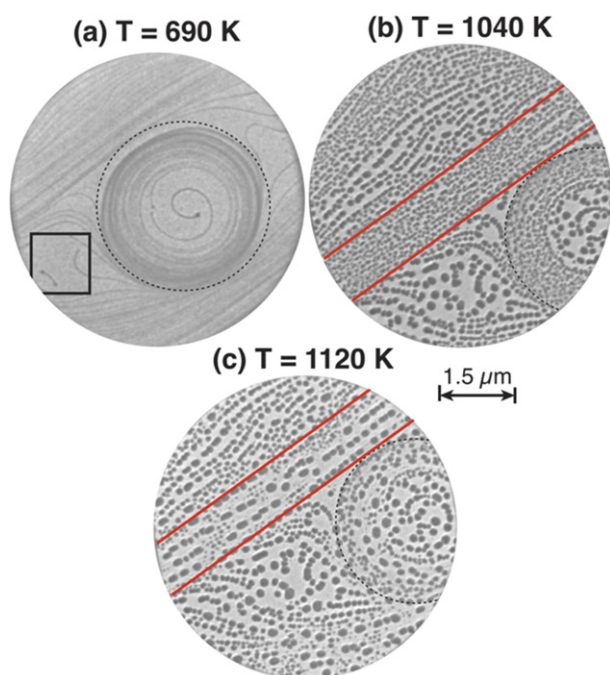


Figure 2. LEEM images during the preparation of $\text{CeO}_2(111)$ islands on $\text{Rh}(111)$. See supporting information for the full movie of the growth process. Reprinted with permission from [17]. Copyright (2014) American Chemical Society.

The most stable termination of CeO_2 is the oxygen terminated (111) plane. This has been prepared on a wide variety of supports as films and nanoscale ‘islands’ including $\text{Ru}(0001)$ [15], $\text{Pt}(111)$ [16], $\text{Rh}(111)$ [17], $\text{Ni}(111)$ [18], Au [19], $\text{Cu}(111)$ [1], $\text{Re}(0001)$ [20] and Pd [21]. Figure 1 shows micrographs and associated low energy electron diffraction (LEED) patterns of ceria islands prepared on a wide range of substrates and shows some of the morphological variations

due to the influence of the support. Key attributes of the support that influence the ceria include the propensity for alloying with Ce (Pt, Rh), the tendency of oxide formation (Ni, Cu) and the strain between the metal and $\text{CeO}_2(111)$ due to lattice mismatch, as indicated in figure 1.

Ultrathin ceria layers of up to tens of nanometres thickness can be formed with good crystallinity on many metal supports. This is usually achieved via physical vapour deposition of cerium metal, followed by oxidation and annealing steps to order and control the stoichiometry of the resultant structures. Fine control of the deposition rate, temperature, and oxygen partial pressure is critical to the final film structure and has been extensively reviewed in the literature [22].

2. Imaging and structure of ceria surfaces

A wide range of experimental techniques have been used to characterise ceria surfaces during and after their preparation. X-ray photoelectron spectroscopy (XPS) is the standard technique for quantifying the oxidation state of the cerium, typically probing the 3d and 4d core levels [22–26]. Resonant photoemission (RESPES) has been used to great effect to study minor changes to the $\text{Ce}^{4+}/\text{Ce}^{3+}$ ratio with very high surface sensitivity [27–29]. Synchrotron soft x-ray absorption spectroscopy has also been used to probe the Ce $M_{4,5}$ absorption edge, which is also sensitive to oxidation state changes of the cerium and provides a more bulk-sensitive measurement [30, 31].

A popular approach to study the larger scale structure of ceria films and nanostructures has been LEEM and the complementary technique of x-ray photoemission electron microscopy (XPEEM). LEEM/XPEEM are full-field microscopy techniques with an ultimate resolution $<10 \text{ nm}$ and can be applied *in situ* in a range of experimental conditions, including during the initial cerium deposition stage

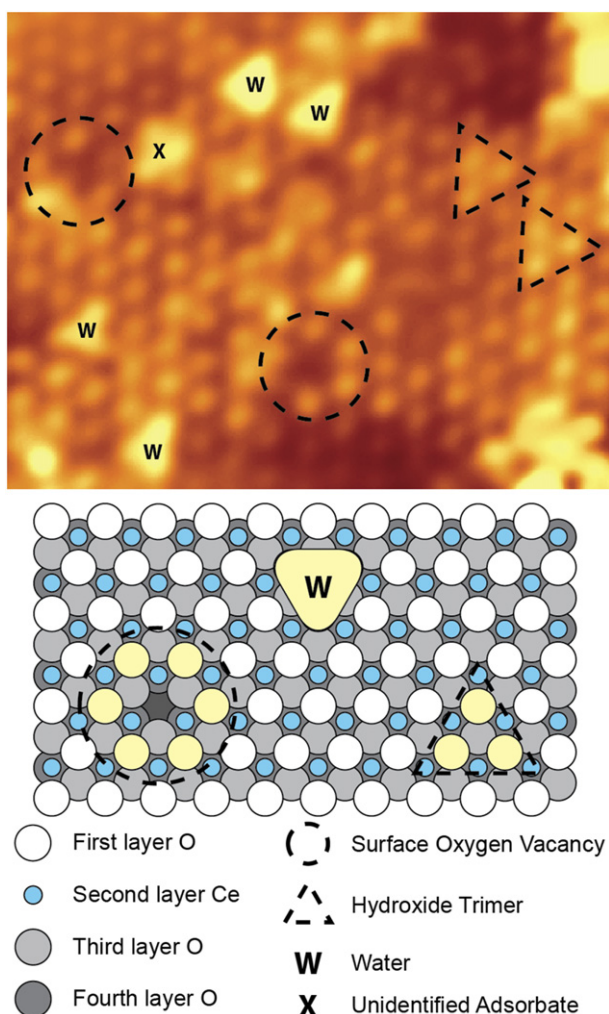


Figure 3. Atomically-resolved STM image of CeO₂(111)/Pt(111). Reprinted with permission from [16]. Copyright (2010) American Chemical Society.

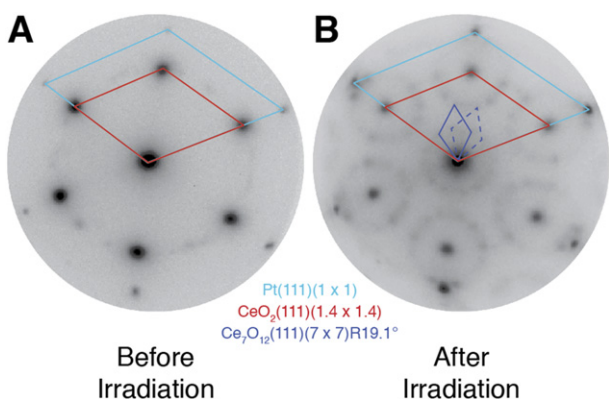


Figure 4. LEED patterns of CeO₂(111) films before and after irradiation with high-flux soft x-rays (~120 eV). Reprinted with permission from [56]. Copyright (2016) American Chemical Society.

and subsequent thermal treatments [32, 33]. As it is a diffractive imaging technique, LEEM instruments can also provide localised LEED measurements of small sample regions (few hundred nm) and more detailed structural information

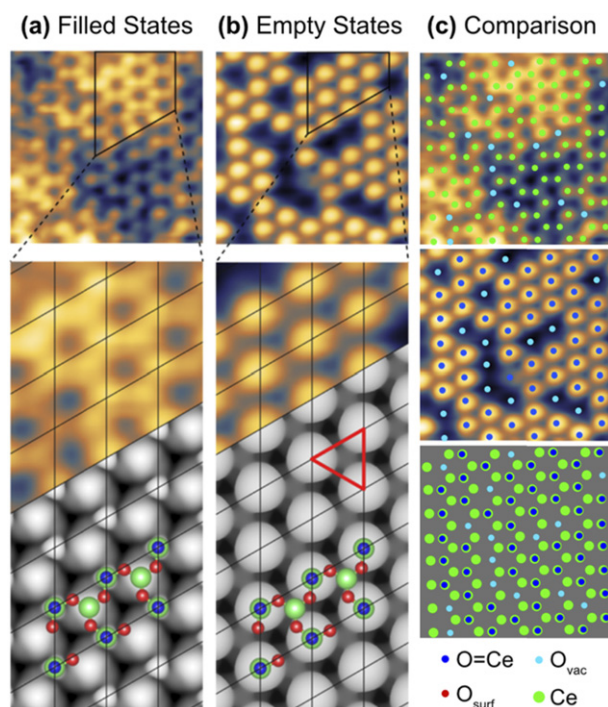


Figure 5. (a) Filled (+1.7 V) and (b) empty (−4 V) states STM images (colour, upper panels) and simulations (monochrome, lower panels) of a Ce=O terminated CeO₂(111)-(√3 × √3)R30° film. The origins of the bright protrusions in the STM images are indicated and compared in (c), highlighting some surface oxygen vacancies (light blue) and the Ce=O species (dark blue). The structural model used for the DFT-simulation is shown in (a) and (b) with green representing Ce, red the surface O, and blue the Ce=O. Reproduced from [51]. CC BY 4.0.

through I-V LEEM measurements [34]. XPEEM combines the high resolution imaging capability of LEEM with elemental and chemical sensitivity via photoemission and absorption processes, as will be discussed later in this topical review.

A key strength of LEEM when applied to the preparation of ceria and other oxide films is the ability to image an area of tens of nanometre in diameter with high spatial resolution (<5 nm) even at elevated temperatures [33, 35, 36]. In the case of the formation of ceria nano-islands on Rh(111), bright-field LEEM imaging was used during the post-deposition oxidation process. Figure 2 shows a series of snapshots (6 μm field of view) taken at different stages of the temperature ramp of ~1 MLE cerium/Rh(111) in 1 × 10^{−7} mbar O₂ [17]. In the first image, figure 2(a) the contrast is just from the Rh(111) surface where the step edges have clear contrast and the deposited cerium is not resolved. As the temperature is increased, figures 2(b) and (c), dark ceria islands are observed to form and ripen, with their morphology clearly influenced by the support structure. The full movie of this process is available in the supporting information (<https://stacks.iop.org/JPCM/34/253001/mmedia>).

The ultimate experimental tool to probe the atomic scale structure and interactions with adsorbates is scanning probe microscopy. Both scanning tunnelling microscopy (STM) and non-contact atomic force microscopy (NC-AFM) have

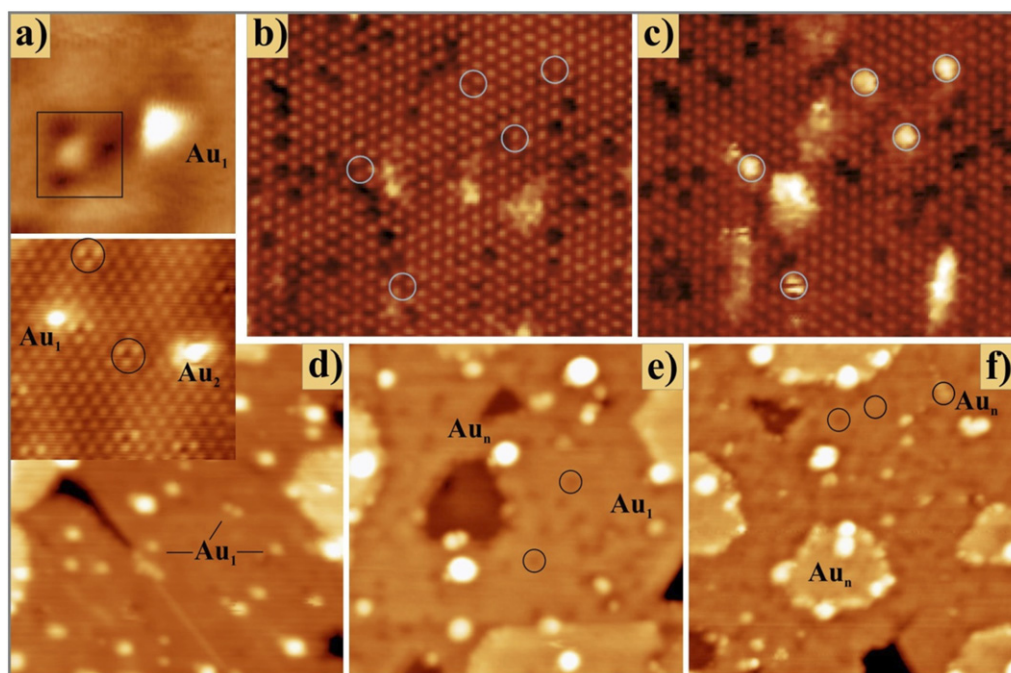


Figure 6. STM images of gold atoms and clusters on partially-reduced ceria surfaces. (a) A regular and defect-bound (square box) Au atom on $\text{CeO}_{2-x}/\text{Ru}(0001)$; (b) and (c) Areas of $\text{CeO}_2(111)-(\sqrt{3} \times \sqrt{3})\text{R}30^\circ$ before and after Au deposition (white circles show adsorption sites); (d) Au deposited on $\text{CeO}_{2-x}/\text{Ru}(0001)$ at 15 K and then annealed to 200 K (e) and 400 K (f). (Black circles highlight defect sites.) Reprinted figure with permission from [15], Copyright (2016) by the American Physical Society.

been extensively applied to ceria single crystals and ultrathin film surfaces for over two decades [37–41]. Despite some high resolution imaging of single crystal CeO_2 , investigations on thin films have proved more popular due to their relative ease of study, particularly at low temperatures. As an extremely sensitive real-space imaging technique, STM has proved particularly well-suited to probing the defect structure of $\text{CeO}_2(111)$ surfaces [16, 42] as illustrated in figure 3. Figure 3 is an atomically-resolved filled states (bright lattice points are located at the top layer oxygen atoms) image of ultrathin film $\text{CeO}_2(111)/\text{Pt}(111)$ with a number of point defects visible including surface oxygen vacancies and water molecules adsorbed from the background vacuum [16]. Comparison of these images with similar NC-AFM studies on single crystal $\text{CeO}_2(111)$ demonstrated the validity of the thin film as a model for the (1×1) surface [16, 43]. Such imaging is now relatively routine at both room temperature and cryogenic temperatures, where scanning tunnelling spectroscopy has also been employed to study the local electronic structure of the stoichiometric surface and around defect sites [42, 44, 45]. The behaviour of such defects, especially oxygen vacancies, is clearly crucial to the oxygen chemistry of ceria surfaces and as such has been a major focus of both experimental and theoretical studies. Similar studies with NC-AFM, which is less affected by charging than STM, but is experimentally significantly more challenging, has also shown the strength of real-space imaging to identify and study different ceria surface reconstructions [46, 47].

Due to the facile formation of oxygen vacancies in the top and subsurface regions, there have been many experimental observations of stable arrangements of such vacancies

resulting in various surface reconstructions with stoichiometries accommodating varying degrees of reduction from CeO_2 (fully Ce^{4+}) to Ce_2O_3 (fully Ce^{3+}) [48–50]. Typically these intermediate reconstructions are prepared by tuning the growth conditions of the ceria layers, the key parameters being oxygen partial pressure (chemical potential) and the temperature [48, 51]. The metal single crystal support and its interface with the ceria is also critical to the formation of these metastable reconstructions [23, 52, 53]. In some cases, post-growth treatments have been used to induce such reconstructions, such as vacuum annealing [54], deposition of metallic cerium [49], or exposure to other reducing agents e.g. hydrogen [55]. Figure 4 shows LEED patterns depicting the transformation of $\text{CeO}_2(111)$ to $\text{CeO}_{2-x}(111)$ via irradiation with soft x-rays (~ 120 eV, highly-focussed undulator beamline source) [56]. After just a few seconds these x-rays, tuned to the Ce 4d–4f absorption leading to a very high absorption cross-section, formed ordered vacancies. The associated reconstruction had a stoichiometry and symmetry of $\text{Ce}_7\text{O}_{12}(111)(7 \times 7)\text{R}19.1$ relative to the $\text{CeO}_2(111)(1.4 \times 1.4)$ and the underlying $\text{Pt}(111)(1 \times 1)$ support. Such synchrotron beam-induced changes have been widely reported for oxide surfaces [57, 58] and illustrate some of the experimental challenges which exist when trying to study redox processes on these materials.

The oxygen chemistry of ceria surfaces is clearly of great importance considering its role in oxygen storage and release in heterogeneous catalysis, and novel surface reconstructions often display interesting bonding structures. Figure 5 shows atomically-resolved STM images (top panels) of a reconstructed $\text{CeO}_2(111)-(\sqrt{3} \times \sqrt{3})\text{R}30^\circ$ film prepared on $\text{Pt}(111)$ under oxygen-lean conditions. Empty (a) and filled (b) states

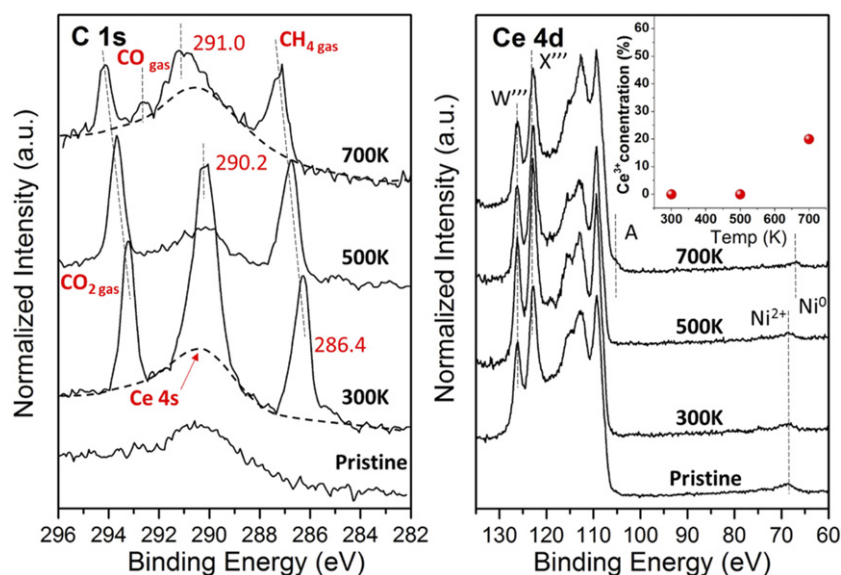


Figure 7. Reactivity of Ni-CeO₂(111) from AP-XPS. C 1s and Ce 4d core levels were measured under UHV (pristine) and when exposed to 100 Torr CO₂ + 100 Torr CH₄ at 300, 500 and 700 K. [24] John Wiley & Sons. © 2016 WILEY-VCH Verlag GmbH & Co. KGaA, Weinheim.

STM images were obtained simultaneously and showed an excellent match to DFT simulations. The registry of the empty and filled states images suggested a novel termination with O atop Ce, that is a rare Ce=O species. This was confirmed by comparison with DFT calculations and high resolution electron energy loss spectroscopy measurements which detected a characteristic Ce=O stretch [51].

3. Supported metals and reactivity

The interaction of metal adatoms and nanoparticles with oxide supports such as ceria has been under intense study for many years, probing key issues such as nucleation, stabilisation under reaction conditions, charge states, metal-support interactions, and deactivation mechanisms [59–62]. Ceria-supported noble metal particles, in particular gold, have attracted much attention due to their catalytic activity in applications such as water-gas-shift and CO oxidation [63–65]. For many metals, including Au, Ag, Pt and Pd, charge transfer from the ceria to the metal has been observed using photoelectron spectroscopy, leading to partial reduction of Ce⁴⁺ to Ce³⁺ at the surface in line with DFT calculations [27, 66–69]. The combination of STM and DFT is a powerful method to directly probe the influence of surface defects on the adsorption behaviour of Au on slightly reduced ceria surfaces, as shown in the work of Lustemberg *et al* [15]. Figure 6 shows STM images of two types of partially-reduced ceria surfaces: (b) and (c) from a reconstructed CeO₂(111)-(√3 × √3)R30° surface, and (a), (d)–(f) from CeO_{2-x}(111)-(1 × 1). For the CeO₂(111)-(√3 × √3)R30° surface, figure 6(b) is the as-prepared surface with a number of dark depressions indicative of surface oxygen vacancies. Figure 6(c) shows the same region after deposition of Au at 300 K (1–3 Au atoms per cluster marked with white circles)—by comparison with the image in (b) there is no clear preference for nucleation at the surface defect sites.

Figure 6(a) shows images of defect bound (black square) and regular Au₁ atoms on CeO_{2-x}(111)-(1 × 1). Figures 6(d)–(f) show the same surface at 15 K, 200 K and 400 K respectively, with surface vacancies highlighted with black circles. Again, there is no clear preference for adsorption at the surface defect sites even as the temperature is increased. Instead, the step edges of the ceria act as trapping sites. This leads to their decoration with larger Au clusters than on the as-deposited surface. The latter, which is shown in figure 6(d), consists mainly of single Au atoms evenly distributed across the film. To understand this somewhat surprising behaviour, DFT was used to calculate the adsorption energies of the various surface sites of these ceria surfaces and also the kinetics of surface diffusion. Although the defect sites are thermodynamically favoured, their population is kinetically hindered by the presence of a significant barrier resulting from the strong diabatic character of the diffusion process. On the stoichiometric surface, Au single atoms were shown to keep a constant 1+ charge, and the barriers towards surface diffusion are relatively small, however since further electron exchange with nearby Ce³⁺ ions is required to populate an oxygen vacancy, this process is kinetically blocked [15]. This result shows the complex nature of the interactions between reducible oxide surfaces and metallic adsorbates, even under carefully controlled ultrahigh vacuum conditions.

There has been a drive towards *in situ* spectroscopic studies of metal nanoparticles supported on ceria surfaces to investigate changes to both metal and ceria during exposure to elevated temperatures and pressures closer to those experienced in industrial catalysts. One key technique here is ambient pressure x-ray photoelectron spectroscopy (AP-XPS), which permits XPS measurements up to tens of mbar, and is now readily available at synchrotron light sources and home laboratories around the world [70, 71]. One system that has been extensively studied using AP-XPS is that of low coverage

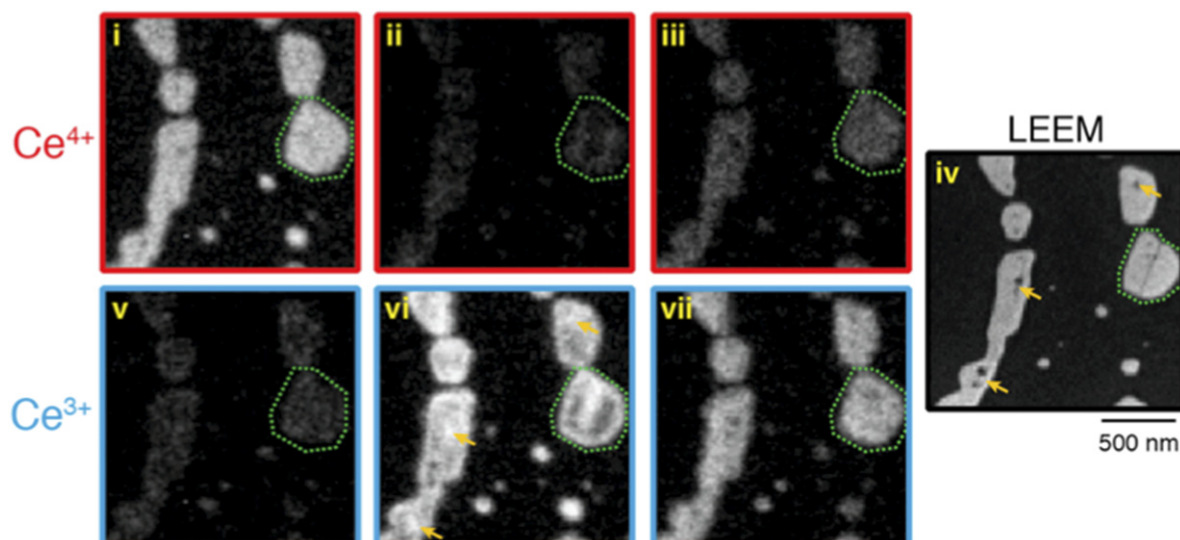


Figure 8. *In situ* resonant micro-XPS following the soft x-ray induced reduction of CeO₂(111) islands supported on Rh(111). Reprinted with permission from [56]. Copyright (2016) American Chemical Society.

Ni nanoparticles on CeO₂(111)/Ru(0001). Well-ordered ceria films, completely covering the Ru surface form the oxide support upon which ~ 0.1 ML Ni was evaporated and annealed in vacuum to prepare the catalyst, with nanoparticles of ~ 2 nm diameter. One key application of this catalyst is methane reforming with CO₂ to form syngas ($\text{CH}_4 + \text{CO}_2 \rightarrow 2\text{CO} + 2\text{H}_2$), where it aids the low temperature activation of the C–O and C–H bonds in the reactants [2, 4, 24, 70, 72]. Figure 7 shows the behaviour of the Ni-CeO₂(111) catalyst under 100 mTorr CH₄ + 100 mTorr CO₂ as the temperature of the system is increased to the operating conditions (700 K) [24]. The C 1s region is dominated by gas phase contributions from the reagents as well as an intermediate activated CO_x species at 300 K which is a result of room temperature activation of the methane. As the temperature is increased, this desorbs from the surface and under reaction conditions some CO gas phase product can even be observed. The Ni nanoparticles remain as 2+ until 700 K, where they are reduced to metallic Ni. The oxidation state of the Ce remains mainly 4+ until 700 K, where significant Ce³⁺ formation is observed.

Correlating structure and reactivity of ceria surfaces is another major aim of the surface science approach to studying these materials. The chemical sensitivity of XPEEM, allowing element-and oxidation state specific imaging up to a few Hz acquisition rates has given us new insights into various redox processes on ceria inverse model catalysts [17, 20, 31, 56]. Figure 8 illustrates how the local reduction of ceria islands can be tracked in real time while the soft x-ray beam reduces the top surface of the ceria [56]. Using resonant energy-selected imaging it is possible to make maps of Ce⁴⁺ (red, panels (i)–(iii)) and Ce³⁺ (blue, panels (v)–(vii)) and compare it to the structure observed in LEEM (panel (iv)). As the reduction proceeds ((i)–(iii), and (v)–(vii)) over a couple of minutes, there is a clear decrease in intensity of Ce⁴⁺ and concomitant increase in Ce³⁺, with the reaction happening most readily at the edges of the islands and at defect sites. (In this

case step edges and holes within the islands.) The combination of LEEM, LEED and XPEEM in a single instrument also permitted the study of the reverse of this process; during the formation of the ceria, an activated (2 × 2) oxygen overlayer was formed on the Rh(111) support in between the islands. By gently heating (~ 400 K) the beam-altered surface, this oxygen was able to reverse spillover onto the ceria, reoxidising it, and showing the complex interplay between the oxide and the metal (Rh).

4. Future outlook

While characterisation of model CeO₂ systems in UHV conditions has now achieved a good degree of maturity, studies at ambient pressure using a number of techniques have much to offer of relevance to catalysis. In particular, AP-PES could be further exploited to investigate surfaces under conditions closer to those employed in catalysis, including recent instrument developments permitting XPEEM measurements in the mbar regime [73]. Methods are also being developed to run PES measurements at significantly higher pressures, such as above 1 bar. These use reaction cells sealed by, for instance, graphene membranes which are photoelectron transparent [74]. Ambient pressure scanning probe microscopy offers a means to follow the morphology of metal nanoparticles as a reaction to gas phase species. It has previously found application in the study of inverse model ceria catalysts supported on Cu(111) [75].

Reflection absorption infrared spectroscopy has previously been used under UHV conditions to monitor adsorption sites of CO on supported Pd on CeO₂ ultrathin films [76]. Because RAIRS is a photon in-photon out technique it can also operate at elevated pressures, which has been exploited in studies of ethanol steam reforming over Ni-CeO₂(111) [77]. Measurements of the dynamics of catalytic reactions are now becoming possible through the advent of fs pulsed x-ray sources in the form of x-ray free electron lasers [78]. Such studies present an

unprecedented opportunity to evaluate reaction mechanisms in exquisite detail sufficient to inform future catalyst design.

Acknowledgments

This work was supported by the European Research Council Advanced Grant ENERGYSURF (GT), European Cooperation in Science and Technology Action CM1104, the EPSRC through Grant EP/L015277/1, the Royal Society through a Wolfson Merit Award to GT, and the Alexander von Humboldt Stiftung.

Data availability statement

No new data were created or analysed in this study.

ORCID iDs

David C Grinter  <https://orcid.org/0000-0001-6089-119X>

Geoff Thornton  <https://orcid.org/0000-0002-1616-5606>

References

- [1] Liu Z *et al* 2020 *Science* **368** 513–7
- [2] Lustemberg P *et al* 2018 *J. Am. Chem. Soc.* **140** 7281–687
- [3] Palomino R M *et al* 2017 *ACS Sustainable Chem. Eng.* **5** 10783–91
- [4] Liu Z *et al* 2017 *Angew. Chem., Int. Ed.* **56** 13041–6
- [5] Liu Z *et al* 2015 *J. Catal.* **321** 90–9
- [6] Grinter D C, Park J B, Agnoli S, Evans J, Hrbek J, Stacchiola D J, Senanayake S D and Rodriguez J A 2015 *Surf. Sci.* **650** 34–9
- [7] Cormack A N, Lamphier S, Wang B, Gubb T and Reed K 2016 *Proc. R. Soc. A* **471** 20150218
- [8] Gorte R J 2010 *AIChE J.* **56** 1126–35
- [9] Wachsman E D and Lee K T 2011 *Science* **334** 935–9
- [10] Trovarelli A, de Leitenburg C, Boaro M and Dolcetti G 1999 *Catal. Today* **50** 353–67
- [11] Mullins D R 2015 *Surf. Sci. Rep.* **70** 42–85
- [12] Rodriguez J A, Liu P, Graciani J, Senanayake S D, Grinter D C, Stacchiola D, Hrbek J and Fernández-Sanz J 2016 *J. Phys. Chem. Lett.* **7** 2627–39
- [13] Novotny Z, Netzer F P and Dohnálek Z 2015 *ACS Nano* **9** 8617–26
- [14] Lykhach Y, Staudt T, Vorokhta M, Skála T, Johánek V, Prince K C, Matolín V and Libuda J 2012 *J. Catal.* **285** 6–9
- [15] Lustemberg P G, Pan Y, Shaw B-J, Grinter D, Pang C, Thornton G, Pérez R, Ganduglia-Pirovano M V and Nilus N 2016 *Phys. Rev. Lett.* **116** 236101
- [16] Grinter D C, Ithnin R, Pang C L and Thornton G 2010 *J. Phys. Chem. C* **114** 17036–41
- [17] Grinter D C, Muryn C, Santos B, Shaw B-J, Menteş T O, Locatelli A and Thornton G 2014 *J. Phys. Chem. C* **118** 19194–204
- [18] Mullins D R, Radulovic P V and Overbury S H 1999 *Surf. Sci.* **429** 186–98
- [19] Ma T, Surnev S and Netzer F 2015 *Materials* **8** 5205–15
- [20] Grinter D C, Yim C-M, Pang C L, Santos B, Menteş T O, Locatelli A and Thornton G 2013 *J. Phys. Chem. C* **117** 16509–14
- [21] Alexandrou M and Nix R M 1994 *Surf. Sci.* **321** 47–57
- [22] Rodriguez J A, Grinter D C, Liu Z, Palomino R M and Senanayake S D 2017 *Chem. Soc. Rev.* **46** 1824–41
- [23] Pagliuca F, Luches P and Valeri S 2013 *Surf. Sci.* **607** 164–9
- [24] Liu Z *et al* 2016 *Angew. Chem., Int. Ed.* **55** 7455–9
- [25] Bagus P S, Nelin C J, Al-Salik Y, Ilton E S and Idriss H 2016 *Surf. Sci.* **643** 142–9
- [26] Allahgholi A, Flege J I, Thiess S, Drube W and Falta J 2015 *ChemPhysChem* **16** 1083–91
- [27] Matharu J, Cabailh G, Lindsay R, Pang C L, Grinter D C, Skála T and Thornton G 2011 *Surf. Sci.* **605** 1062–6
- [28] Grinter D C, Graciani J, Palomino R M, Xu F, Waluyo I, Sanz J F, Senanayake S D, Rodriguez J A and Rodriguez J A 2021 *Surf. Sci.* **710** 121852
- [29] Staudt T, Lykhach Y, Tsud N, Skála T, Prince K C, Matolín V and Libuda J 2010 *J. Catal.* **275** 181–5
- [30] Allan M, Grinter D, Dhaliwal S, Muryn C, Forrest T, Maccherozzi F, Dhési S S and Thornton G 2019 *Surf. Sci.* **682** 8–13
- [31] Grinter D C, Pang C L, Muryn C A, Maccherozzi F, Dhési S S and Thornton G 2014 *J. Electron Spectrosc. Relat. Phenom.* **195** 13–7
- [32] Grinter D C and Thornton G 2018 Characterization Tools for Ultrathin Metal Oxides *Encyclopedia of Interfacial Chemistry: Surface Science and Electrochemistry* ed K Wandelt (Amsterdam: Elsevier)
- [33] Flege J I and Grinter D C 2018 *Prog. Surf. Sci.* **93** 21–45
- [34] Flege J I, Kaemena B, Meyer A, Falta J, Senanayake S D, Sadowski J T, Eithiraj R D and Krasovskii E E 2013 *Phys. Rev. B* **88** 235428
- [35] Höcker J *et al* 2017 *Phys. Chem. Chem. Phys.* **19** 3480–5
- [36] Grinter D C, Senanayake S D and Flege J I 2016 *Appl. Catal., B* **197** 286–98
- [37] Nörenberg H and Briggs G A D 1997 *Phys. Rev. Lett.* **79** 4222–5
- [38] Esch F, Fabris S, Zhou L, Montini T, Africh C, Fornasiero P, Comelli G and Rosei R 2005 *Science* **309** 752–5
- [39] Eck S, Castellarin-Cudia C, Surnev S, Ramsey M G and Netzer F P 2002 *Surf. Sci.* **520** 173–85
- [40] Castellarin-Cudia C, Surnev S, Schneider G, Podlucky R, Ramsey M G and Netzer F P 2004 *Surf. Sci.* **554** 120–6
- [41] Gritschneider S, Namai Y, Iwasawa Y and Reichling M 2005 *Nanotechnology* **16** 41–8
- [42] Jerratsch J-F, Shao X, Nilus N, Freund H-J, Popa C, Ganduglia-Pirovano M V, Burow A M and Sauer J 2011 *Phys. Rev. Lett.* **106** 246801
- [43] Gritschneider S and Reichling M 2007 *Nanotechnology* **18** 044024
- [44] Pan Y, Cui Y, Stiehler C, Nilus N and Freund H-J 2013 *J. Phys. Chem. C* **117** 21879–85
- [45] Shao X, Jerratsch J-F, Nilus N and Freund H-J 2011 *Phys. Chem. Chem. Phys.* **13** 12646–51
- [46] Torbrugge S, Reichling M, Ishiyama A, Morita S and Custance O 2007 *Phys. Rev. Lett.* **99** 056101
- [47] Olbrich R, Murgida G E, Ferrari V, Barth C, Llois A M, Reichling M and Ganduglia-Pirovano M V 2017 *J. Phys. Chem. C* **121** 6844–51
- [48] Höcker J, Duchoň T, Veltruská K, Matolín V, Falta J, Senanayake S D and Flege J I 2016 *J. Phys. Chem. C* **120** 4895–901
- [49] Duchon T *et al* 2014 *J. Phys. Chem. C* **118** 357–65
- [50] Stetsovych V *et al* 2013 *J. Phys. Chem. Lett.* **4** 866–71
- [51] Grinter D C *et al* 2021 *Angew. Chem., Int. Ed.* **60** 13835–9
- [52] Flege J I *et al* 2016 *Nanoscale* **8** 10849–56
- [53] Sauerbrey M, Gasperi G, Luches P, Falta J, Valeri S and Flege J I 2017 *Top. Catal.* **60** 513–21
- [54] Wilkens H *et al* 2013 *Phys. Chem. Chem. Phys.* **15** 18589–99
- [55] Höcker J, Menteş T O, Sala A, Locatelli A, Schmidt T, Falta J, Senanayake S D and Flege J I 2015 *Adv. Mater. Interfaces* **2** 1500314

- [56] Grinter D C, Murny C, Sala A, Yim C-M, Pang C L, Mentes T O, Locatelli A and Thornton G 2016 *J. Phys. Chem. C* **120** 11037–44
- [57] Pang C L and Thornton G 2015 *Photon-, Electron-, and Scanning Tunneling Microscopy-Induced Defects on Oxide Surfaces in Defects in Oxide Surfaces* ed J Jupille and G Thornton (Berlin: Springer)
- [58] Gregoratti L, Mentes T O, Locatelli A and Kiskinova M 2009 *J. Electron Spectrosc. Relat. Phenom.* **170** 13–8
- [59] Pacchioni G and Freund H-J 2018 *Chem. Soc. Rev.* **47** 8474–502
- [60] Freund H-J 2016 *J. Am. Chem. Soc.* **138** 8985–96
- [61] Cargnello M, Doan-Nguyen V V T, Gordon T R, Diaz R E, Stach E R, Gorte R, Fornasiero P and Murray C 2013 *Science* **341** 771–3
- [62] Neitzel A *et al* 2016 *J. Phys. Chem. C* **120** 9852–62
- [63] Fu Q, Saltsburg H and Flytzani-Stephanopoulos M 2003 *Science* **301** 935–8
- [64] Guzman J, Carretin S, Fierro-Gonzalez J C, Hao Y, Gates B C and Corma A 2005 *Angew. Chem.* **117** 4856–9
- [65] Rodriguez J A 2011 *Catal. Today* **160** 3–10
- [66] Luches P, Pagliuca F, Valeri S, Illas F, Preda G and Pacchioni G 2012 *J. Phys. Chem. C* **116** 1122–32
- [67] Pan Y, Nilius N, Freund H-J, Paier J, Penschke C and Sauer J 2013 *Phys. Rev. Lett.* **111** 206101
- [68] Wilson E L *et al* 2008 *J. Phys. Chem. C* **112** 10918–22
- [69] Wilson E L, Chen Q, Brown W A and Thornton G 2007 *J. Phys. Chem. C* **111** 14215–22
- [70] Palomino R M, Hamlyn R, Liu Z, Grinter D C, Waluyo I, Rodriguez J A and Senanayake S D 2017 *J. Electron Spectrosc. Relat. Phenom.* **221** 28–43
- [71] Head A and Bluhm H 2018 Ambient Pressure X-Ray Photoelectron Spectroscopy *Encyclopedia of Interfacial Chemistry* ed K Wandelt (Amsterdam: Elsevier)
- [72] Lustemberg P G, Ramirez P J, Liu Z, Gutiérrez R A, Grinter D G, Carrasco J, Senanayake S D, Rodriguez J A and Ganduglia-Pirovano M V 2016 *ACS Catal.* **6** 8184–91
- [73] Ning Y, Fu Q, Li Y, Zhao S, Wang C, Breitschaft M, Hagen S, Schaff O and Bao X 2019 *Ultramicroscopy* **200** 105–10
- [74] Weatherup R S, Eren B, Hao Y, Bluhm H and Salmeron M B 2016 *J. Phys. Chem. Lett.* **7** 1622–7
- [75] Graciani J *et al* 2014 *Science* **345** 546–50
- [76] Wilson E L, Brown W A and Thornton G 2006 *Surf. Sci.* **600** 2553–61
- [77] Liu Z *et al* 2016 *Phys. Chem. Chem. Phys.* **18** 16621–8
- [78] Dell’Angela M *et al* 2013 *Science* **339** 1302–5